

PAPER • OPEN ACCESS

Spectral investigations of low-temperature plasma induced in CO₂ gas by nanosecond pulses of extreme ultraviolet (EUV)

To cite this article: A Bartnik *et al* 2021 *Plasma Sources Sci. Technol.* **30** 115008

View the [article online](#) for updates and enhancements.

You may also like

- [Thermalization of electrons in decaying extreme ultraviolet photons induced low pressure argon plasma](#)
J Beckers, R M van der Horst, E A Osorio et al.
- [Exploring the electron density in plasma induced by EUV radiation: II. Numerical studies in argon and hydrogen](#)
D I Astakhov, W J Goedheer, C J Lee et al.
- [Mapping electron dynamics in highly transient EUV photon-induced plasmas: a novel diagnostic approach using multi-mode microwave cavity resonance spectroscopy](#)
J Beckers, F M J H van de Wetering, B Platier et al.



Instruments for Advanced Science

- Knowledge,
- Experience,
- Expertise

[Click to view our product catalogue](#)

Contact Hiden Analytical for further details:
www.HidenAnalytical.com
info@hiden.co.uk

Gas Analysis



- dynamic measurement of reaction gas streams
- catalysis and thermal analysis
- molecular beam studies
- dissolved species probes
- fermentation, environmental and ecological studies

Surface Science



- UHV-TPD
- SIMS
- end point detection in ion beam etch
- elemental imaging - surface mapping

Plasma Diagnostics



- plasma source characterization
- etch and deposition process reaction kinetic studies
- analysis of neutral and radical species

Vacuum Analysis



- partial pressure measurement and control of process gases
- reactive sputter process control
- vacuum diagnostics
- vacuum coating process monitoring

Spectral investigations of low-temperature plasma induced in CO₂ gas by nanosecond pulses of extreme ultraviolet (EUV)

A Bartnik^{*}, W Skrzeczanowski, P Wachulak, T Fok, Ł Węgrzyński, M Szczurek and H Fiedorowicz

Institute of Optoelectronics, Military University of Technology, Warsaw, Poland

E-mail: andrzej.bartnik@wat.edu.pl

Received 18 May 2021, revised 2 September 2021

Accepted for publication 11 October 2021

Published 5 November 2021



Abstract

In this work, low-temperature plasmas, induced in a gaseous CO₂ by intense extreme ultraviolet (EUV) pulses were investigated with a purpose to determine their ionic/molecular composition and the resulting, potentially reactive species. Two laser-produced plasma EUV sources based on a xenon gas puff target were used to irradiate and ionize of the CO₂ gas. The sources, driven by Nd:YAG lasers of different parameters, delivered EUV beams created using reflective, focusing collectors. The CO₂-based, low-temperature plasmas induced using both systems, emitted radiation in a wide wavelength range, from vacuum ultraviolet (VUV) to visible light (VIS). The radiation was measured using spectrometers and a streak camera operating in these spectral ranges. In the VUV range, multiple emission lines corresponding to ionic and atomic species together with the CO molecular bands were acquired. Spectra from the UV–VIS range were mainly composed of the CO₂⁺ molecular bands. Numerical simulations of the molecular spectra allowed us to estimate rotational and vibrational temperatures of the EUV induced plasmas. As could be expected, plasmas created in both experimental systems were characterized by different temperatures and intensity ratios of the ionic–atomic spectral lines. The spatio-temporal measurements performed using the streak camera indicated a few times longer lifetime of the EUV induced plasmas, compared to the driving, EUV pulses.

Keywords: extreme ultraviolet, extreme ultraviolet photoionization, extreme ultraviolet induced plasma, low temperature plasma


(Some figures may appear in colour only in the online journal)

1. Introduction

Energetic photons from soft x-ray (SXR, 0.1–10 nm), extreme ultraviolet (EUV, 10–120 nm), or vacuum ultraviolet (VUV, 100–200 nm) range can induce various atomic processes in

gases. It concerns especially photoionization, photoexcitation, direct or indirect photodissociation. Due to the intense emission of these energetic photons by stars, such processes are common in space, mainly in accretion disks, protoplanetary disks, or upper planetary atmospheres [1–3]. The photon-induced events can result in the formation of so called photoionized plasmas. Some of these plasmas or molecular processes induced in Space by energetic photons were simulated and studied under laboratory conditions. Namely it concerns photoionized plasmas formed in binary systems with a compact star as an intense x-ray source. The corresponding

* Author to whom any correspondence should be addressed.

 Original content from this work may be used under the terms of the [Creative Commons Attribution 4.0 licence](https://creativecommons.org/licenses/by/4.0/). Any further distribution of this work must maintain attribution to the author(s) and the title of the work, journal citation and DOI.

experiments were performed using plasma x-ray sources of high peak power, having spectral distribution close to black-body emission. It required to employ high Z, high temperature plasmas of high density. Plasmas of the necessary parameters were formed in a final stage of high current Z-pinch or laser-driven compression of a spherical pellet. High energy x-ray pulses emitted by these plasmas were used for irradiation of gas embedded in a gas cell [4, 5] or preformed low temperature plasma [6]. In both cases, the irradiated gas media were located in the proximity of x-ray emitting plasmas. In extreme cases, however, the x-ray power densities exceeded $10^{11} \text{ W cm}^{-2}$ allowing to induce photoionized plasmas with high ionization degrees and perform laboratory simulations of photoionized plasmas driven by astrophysical x-ray sources [5].

The above mentioned experiments concerned photoionization of atomic gases or cold plasmas. There were also many experiments concerning low temperature plasmas or processes induced by EUV or VUV photons in molecular gases. The experiments concerned either astrophysical or technological plasmas. One of the laboratory astrophysics experiments was performed with plasmas induced in hydrogen employing a specially prepared converter of the x-ray to the EUV pulse [7]. Using the converter, laboratory simulation of a white dwarf photosphere was performed.

Photoionization of other molecular gases is one of the important processes for planetary science, in particular, it is one of the dominant processes present in upper regions of the planetary atmospheres. Photoionization can result in further dissociation to ionic and neutral species. Ionization of oxygen, nitrogen and other simple molecules by the EUV/VUV solar radiation is one of the important channels of ion production in the upper atmospheres of Earth and Titan [8–10].

Laboratory simulation of these processes or formation of the EUV/VUV induced low temperature plasmas does not require an extremely high radiation field, like in experiments on x-ray induced plasmas performed using high pulsed power facilities. The majority of the Solar electromagnetic radiation is emitted in the EUV/VUV range. Energies of the EUV/VUV photons are sufficient for ionization, excitation, or dissociation of any molecule. Due to comparable photon energies to binding energies of valence electrons, cross-sections for processes induced by EUV/VUV photons are much higher than in the case of x-ray photons [11–14]. In this case, EUV or VUV induced plasmas can be created using the radiation pulses accessible from small-scale laboratory sources, with the radiation power density of the order of $10^7\text{--}10^9 \text{ W cm}^{-2}$ [15–17]. In principle, experiments on laboratory simulation of molecular processes in upper planetary atmospheres were even performed using VUV sources of low power, namely VUV lamps. In these cases, H₂/He lamp (122 nm), Xe lamp (147 nm) both with an MgF₂ window or CH₄/He lamp (193 nm) with a quartz window [18–20] were used.

Investigation of low temperature plasmas, induced in molecular gases by the EUV photons, can be connected also with some technological processes. One of the most important problem concerns plasmas produced in the EUV lithography tools. In this case, plasmas of very low density are created in a vacuum chamber, which is filled with gas to protect the EUV

optical systems, from the effects of debris generated by the EUV source. For such purposes, hydrogen or argon gases are considered [21–23]. These gases are exposed to the EUV photons during the operation of the lithography tool which results in low temperature plasmas with a very low electron density. Measured values of the density in Ar plasmas were of the order of 10^{10} cm^{-3} [24], for the hydrogen plasmas it was even two orders of magnitude lower [22]. Measurements of ion distribution in H₂ based plasmas indicated for creation of H⁺, H₂⁺, and H₃⁺ ionic species [25].

Various EUV induced plasmas were also investigated by the authors of the paper. In these cases, however, the plasma density was much higher, exceeding 10^{17} cm^{-3} [26]. Spectral investigations of these plasmas, in a wide range from SXRs to visible light, were performed. Either emission or absorption spectra were measured. Based on the measurements, ionic composition and plasma parameters were estimated. Plasmas induced in reactive gases were used in various experiments concerning surface processing [27–29].

In this paper results of the spectral investigation of low temperature plasmas induced in CO₂ gas are presented. CO₂ is an inert gas in normal conditions. Irradiation of the gas with intense EUV pulses can convert it to low temperature plasma containing various reactive species. The main goal of the experimental studies was to determine parameters and constituents of the EUV induced, CO₂-based plasmas, using spectral methods. Plasmas were produced by irradiating a small amount of gas, injected under pressure into a vacuum chamber, with nanosecond EUV pulses. For the gas irradiation, two laboratory systems were used, based on laser-produced plasma (LPP) EUV sources, driven by Nd:YAG lasers of different pulse energy and time duration. The parameters of the investigated plasma were estimated on the basis of measurements of molecular spectra and comparison with the results of numerical simulations carried out using the PGOPHER code [30, 31].

2. Experimental arrangements

EUV induced plasmas were produced using two LPP sources delivering EUV pulses of different fluencies. The first one is driven using a 10 Hz Nd:YAG laser (NL 303 HT, EXPLA, Lithuania), generating pulses of energy 0.8 J and pulse duration of 4 ns. The second source employs an Nd:YAG laser system of significantly higher pulse energy up to 10 J (NL 129, EXPLA). The laser pulse duration can be changed within a range of 1–10 ns. Laser pulses are generated with a 10 Hz repetition rate. In both cases, LPPs are created by the interaction of the focused laser beam with a gas puff target. The target is being formed using a specially prepared, electromechanically operated, valve system. The system is equipped with a concentric double nozzle set-up, allowing to inject a high Z gas (usually xenon) into a hollow stream of helium (Xe/He target). Such configuration of the gas injection system prevents a free expansion of the inner gas into a vacuum. Apart from that absorption of EUV photons in the He gas is negligible comparing to self-absorption in neutral or weakly ionized xenon. This type of gaseous target offers a possibility to create

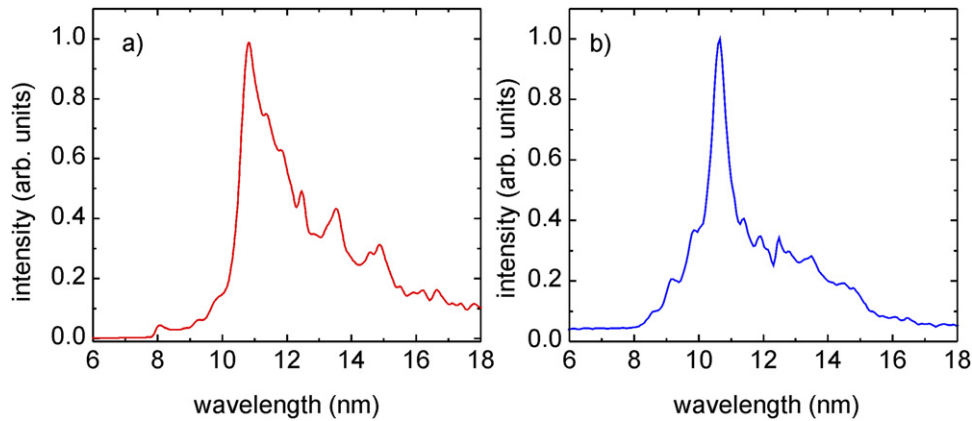


Figure 1. EUV spectra of the focused radiation for LPP EUV sources based on two laser systems: (a) NL 303 HT (0.8 J, 4 ns), (b) NL 129 (5 J, 10 ns).

LPPs at a sufficiently long distance from the nozzle, preventing its erosion by hot plasmas. Lack of self-absorption results in high energy conversion of the laser pulse into the EUV. More detailed description of the source system can be found in various earlier papers, concerning surface processing [32] or SXR and EUV microscopy [33, 34].

Both EUV sources were equipped with identical gold-plated, grazing incidence, ellipsoidal collectors (RITE s.r.o., Czech Republic). The distance between foci of the collector (from LPP to the interaction region) was 300 mm, the LPP was created in one of them, and hence, the EUV radiation was focused in the second focal point. Due to the reflective index limitation for the short-wavelength region, the EUV focusing was effective in the wavelength range $\lambda > 9$ nm. In figure 1 the corresponding EUV spectra of the focused radiation, recorded for both sources, are presented. In both cases, pronounced spectral maxima are at the wavelength $\lambda \cong 10.8$ nm.

There are some differences between the spectral distributions for both sources, however, they are not very significant. The main difference concerns the EUV fluence, which can be obtained in the focal plane of the collectors. It was measured using a system, based on a calibrated pinhole, coupled to an AXUV100 detector, sensitive for the EUV photons [32]. In the case of the EUV source driven by the NL 303 HT laser, the fluence in the central area of the focal spot reached 65 mJ cm^{-2} . The corresponding measurements performed for the second source, based on the NL 129 laser system gave the value 450 mJ cm^{-2} [35]. An FWHM of the intensity distribution across the focal spot was 1.4 mm.

The EUV beam formed this way was used for photoionization of CO_2 gas which was injected into the focal area, orthogonally to an optical axis of the collecting mirror, using an auxiliary gas puff valve. The valve was equipped with a tube-shaped nozzle, with an outlet located 2 mm from the optical axis of the irradiation system. A density of the gas, delivered to the interaction region, could be regulated within the range of approximately 1%–10% of the atmospheric density. In figure 2 the irradiation configuration is presented. A more detailed description of the injection system can be found in reference [36].

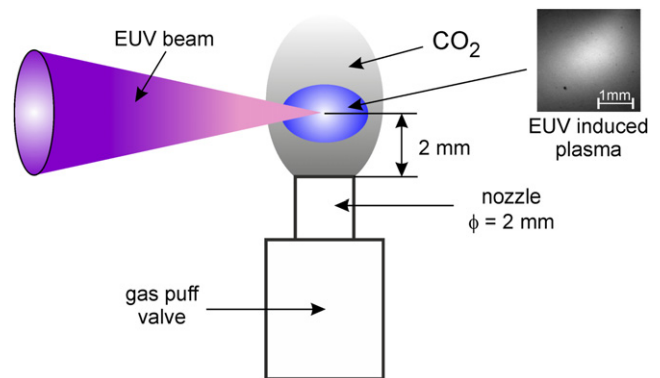


Figure 2. Schematic view of the irradiation geometry, of the CO_2 gas, injected into the vacuum chamber, using an injection system based on a gas puff valve.

Irradiation of CO_2 gas by the intense beam of the EUV photons resulted in generation of low temperature plasmas. Comparative studies of these plasmas were performed by spectral investigations in a VUV ($\lambda = 90\text{--}200$ nm) and UV/VIS ($\lambda = 200\text{--}780$ nm) wavelength ranges. The UV/VIS measurements were carried out, using an Echelle Spectra Analyzer ESA 4000 with a spectral resolution of $\lambda/\Delta\lambda \approx 20000$. For the measurements in the VUV range, the spectrograph from DR. HOERLEIN + PARTNER GbR, based on a concave flat-field varied-linespace grating, having average 1200 grooves/mm, was employed. Its spectral resolution is significantly lower comparing to the UV/VIS spectrograph, approximately $\lambda/\Delta\lambda \approx 500$. The spectra were recorded using a back-illuminated CCD camera (DO920P, Andor) cooled down to a temperature of -60°C .

Additionally, spatio-temporal investigation of the CO_2 -based plasma was performed. The corresponding measurements concerned UV–VIS emission from plasmas formed in the focal region of the EUV beam. The measurements were carried out using an optical streak camera (Hamamatsu C10910). Its optical axis was perpendicular to the axis of the EUV irradiation system. A 2" diameter plano-convex lens with the focal distance $f = 100$ mm was mounted at a distance of 290 mm from the plasma region and 155 mm from the entrance

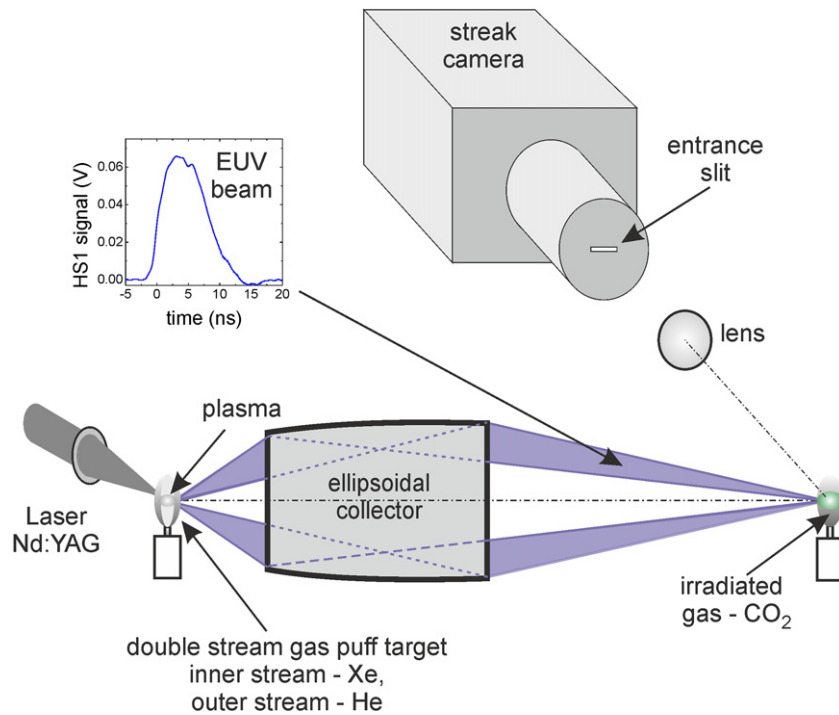


Figure 3. Schematic view of the experimental system with the streak camera for spatio-temporal measurement. For spectral measurements, the camera was replaced by the VUV or UV–VIS spectrometer.

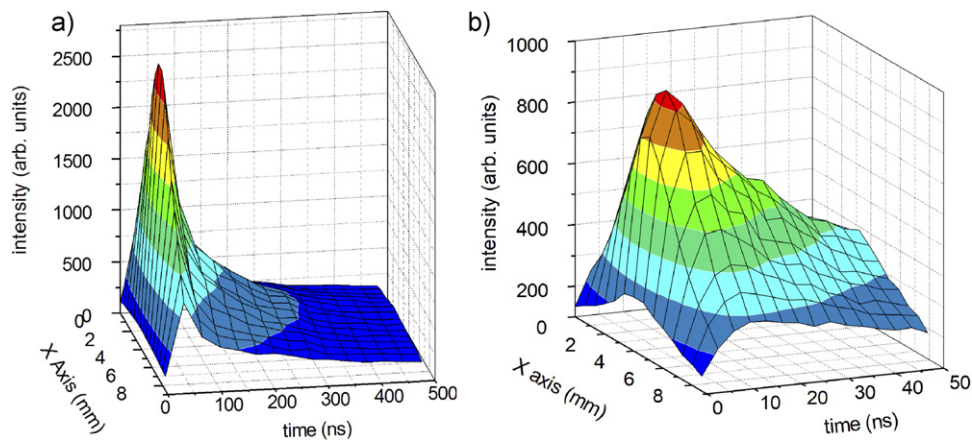


Figure 4. Spatio-temporal intensity profiles obtained from streak images of the optical emission from the EUV induced CO_2 plasmas. Spatial dimension along the optical axis of the irradiating EUV beam. Two streak times: (a) 500 ns, (b) 50 ns.

slit of the camera. It allowed forming the plasma image in the slit plane with the most bright region located at the slit. A schematic view of the experimental arrangement is presented in figure 3.

3. Experimental results

Irradiation of the CO_2 gaseous target, formed inside the vacuum chamber, by intense EUV pulses resulted in partial dissociation and creation of various excited states in neutral or ionic species. The resulting low temperature plasmas were studied by emission spectroscopy in a wide wavelength range $\lambda = 90\text{--}780$ nm. Additionally, it was possible to obtain streak images of the EUV induced plasmas in the UV–VIS range. It

allowed us to estimate the one-dimensional spatial distribution of the brightest emission region with a temporal resolution. Results of the measurements performed for 500 ns and 50 ns streak times are presented in figure 4.

The spatial profile (X axis) corresponds to a one-dimensional image of the plasma formed along the EUV beam, in the focal region. It can be noticed that the plasma size in this direction exceeds 9 mm with the FWHM of the spatial profile approaching 6 mm. The plasma emission in the optical range increases to its maximal value during 10 ns, then decreases slowly to 10% of the maximum value within a time of approximately 300 ns.

Time integrated, spectral investigations were performed using the VUV and UV–VIS spectrographs. Typical VUV

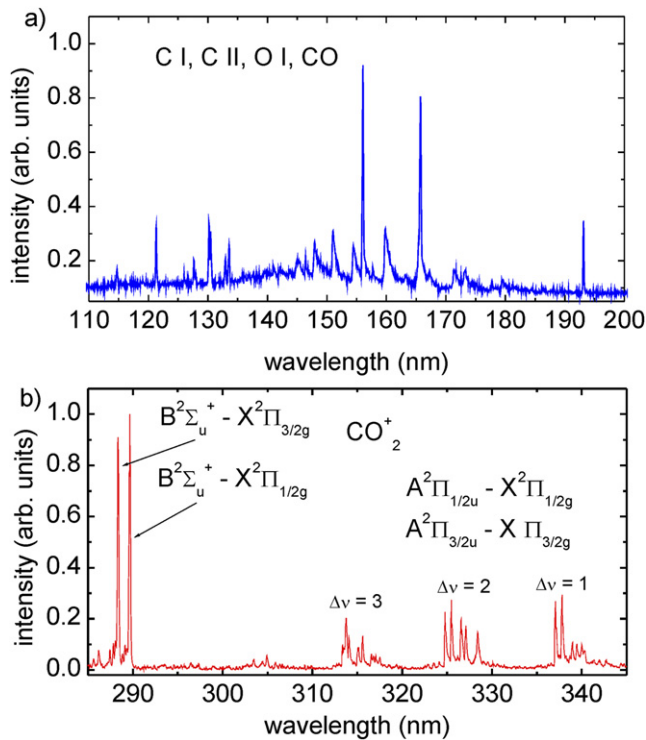


Figure 5. Survey spectra of the CO_2 -based plasma emission recorded using: (a) VUV, (b) UV–VIS spectrometers.

and UV spectra obtained from plasmas, created using the EUV source based on the NL 303 HT laser, are presented in figure 5. The VUV spectrum, shown in figure 5(a), is composed of multiple lines originating from radiative transitions in ionic or atomic species of carbon and oxygen. The most intense are emission lines corresponding to CI, $2s^22p^2-2s2p^3$ ($\lambda = 156$ nm), $2s^22p^2-2s^22p3s$ ($\lambda = 165.7$ nm, 193.1 nm), transitions, however the CII, $2s^22p-2s2p^2$ ($\lambda = 133.5$ nm) and OI, $2s^22p^4-2s^22p^3(^4S^o)3s$ ($\lambda = 130.2$ nm, 130.5 nm) lines are also clearly visible. The spectrum contains also numerous emission features corresponding to spectral bands of $A^1\Pi-X^1\Sigma^+$ fourth positive system of carbon monoxide [37].

The second spectrum (figure 5(b)) is composed of the Fox–Duffendack–Barker $A^2\Pi-X^2\Pi$ band system and the ultraviolet doublet system $B^2\Sigma^+-X^2\Pi$ of CO_2^+ molecular ions [38]. Additionally, outside the presented wavelength range the CI resonance line $2s^22p^2\ ^1S_0-2s^22p3s\ ^1P^o$ was detected.

Similar spectra were obtained from plasmas created using the second EUV source. They contain the same lines and molecular features. The difference can be seen in the UV spectra recorded with high resolution. In this case, the spectral structure of the molecular bands is better visible. In figure 6 the corresponding parts of the CO_2^+ spectra for both irradiation systems are presented. It can be noticed that envelopes of rotational lines have different shapes. In figures 6(b) and (c) these envelopes form double peak structures with pronounced minima between the narrow, intense peaks and wide peaks of a few times lower intensities. The corresponding spectral

features visible in figures 6(e) and (f) do not have these minima. It is even better visible in the spectra obtained from the numerical simulations (figures 8 and 9). Significant differences can be noticed also in the spectral range 288–290 nm for the ultraviolet doublet ($B^2\Sigma_u^+-X^2\Pi_g$). It concerns especially short-wavelength sides (*R*-branch) of the spectral features. Their relative intensities in respect to the central narrow peaks of the features are significantly lower in the spectrum obtained using the irradiation system based on the NL 303 HT laser (figure 6(a)) comparing to the spectrum from the second irradiation system (figure 6(d)).

The difference between spectra recorded using both experimental systems concerns also their intensities. In figure 6 intensities of the corresponding spectral features are comparable. However, it should be noticed, that in the case of the irradiation system based on the NL 303 HT laser, 500 UV pulses were accumulated to obtain the spectrum. In the case of the NL129 laser system accumulation of 10 UV pulses was sufficient. The optical system coupled to the spectrometer in both cases was the same, which means that the difference was connected only with the UV emission from the EUV induced plasmas.

Concerning the spectra recorded in the VUV range, differences in total intensities were similar. Their relative spectral distributions indicate some minor differences except a line corresponding to the radiative transition $2s^22p\ ^2P^o-2s2p^2\ ^2D$ of single charged carbon ions, CII. In the VUV spectrum recorded for the EUV induced plasma created using the first irradiation system, relative intensity of this line is comparable to the adjacent CI line (figure 7(a)). In the spectrum from the second system (figure 7(b)) the CII/CI ratio exceeds 5. It means that the ionization degree was higher in this case, as could be expected.

Analysis of the molecular spectra was based on the available published data and numerical simulations. Identification of the band heads was performed using the corresponding data from reference [39]. The simulations were performed using a PGOPHER code dedicated for simulation of rotational, vibrational, and electronic spectra. Two kinds of molecular species were considered: diatomic, namely CO and three atomic- CO_2^+ . Experimental spectra of the latter molecular ions are presented in figure 8. For numerical simulations of these spectra, some molecular constants were necessary. It concerns especially band origins and rotational constants. For the $X^2\Pi$ states, the corresponding constants were taken from the reference [40]. Origins for the $A^2\Pi$ states were calculated as a sum of the $X^2\Pi$ origins and excitation energies between the corresponding $A^2\Pi_u-X^2\Pi_g$ vibronic states reported in references [41, 42]. The final determination of the origins was performed by the fitting of the simulated to the experimental spectra employing the PGOPHER program. The corresponding molecular constants are gathered in table 1.

The simulated spectra corresponding to the experimental spectra of the Fox–Duffendack–Barker ($A^2\Pi_u-X^2\Pi_g$) system (figures 6(b) and (c)) obtained using the first irradiation system are presented in figure 8. For proper fit of the simulated to the experimental spectra, a Gaussian broadening of the lines was assumed at a level of 0.02 nm which corresponds to the

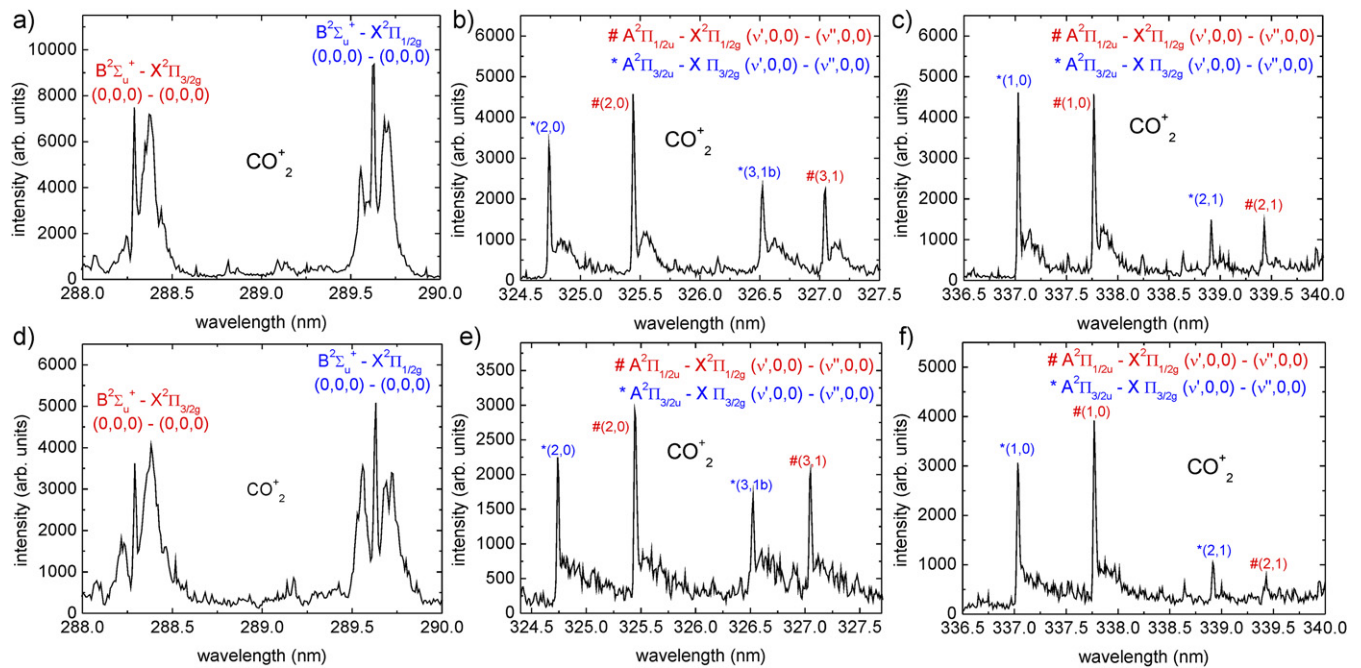


Figure 6. UV–VIS spectra recorded for the EUV induced plasmas using two irradiation systems, based on the NL 303 HT (a)–(c) and NL 129 (d)–(f) laser systems.

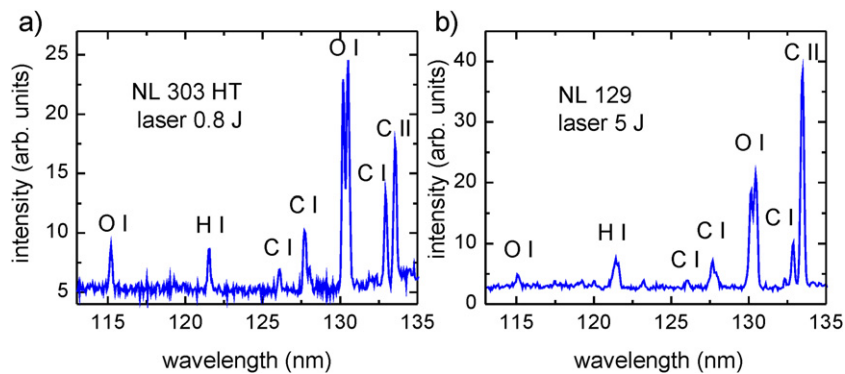


Figure 7. VUV spectra recorded for the EUV induced plasmas using two irradiation systems, based on the NL 303 HT (a) and NL 129 (b) laser systems.

resolution of the spectrometer. Similar simulations were performed for the spectra recorded in the second irradiation system. The results are presented in figure 9.

The PGOPHER code allows performing numerical simulations assuming two different temperatures: vibrational T_v and rotational T_r . In the case of simulations of the emission spectra obtained from plasmas induced using the first irradiation system, a good fit was obtained for $T_v \sim 4000$ K and $T_r \sim 100$ K. For simulations performed for the second system the corresponding values were $T_v \sim 6000$ K and $T_r \sim 180$ K.

A series of numerical simulations, performed with the PGOPHER code, indicate that relative intensities of the spectral features are not very sensitive to changes of the vibrational temperature in a wide range up to $T_v \sim 10^4$ K. A significant influence on the spectra concerned the rotational temperature. It can be noticed that the shapes of the spectral bands obtained for 100 K and 180 K differ significantly. A similar difference is

visible also in the experimental spectra shown in figures 6(b), (c) (e) and (f), respectively.

The PGOPHER code was employed also for numerical simulation of the CO spectra recorded in the VUV range. Origins and rotational constants for the CO, $A^1\Pi - X^1\Sigma^+$ system were calculated using the corresponding formulas for linear molecules [43] and the necessary data from the NIST database [44]. In figure 10 a part of the VUV experimental spectrum recorded using the experimental system based on the NL129 laser, together with the simulated spectrum is presented.

Simulations were performed for various temperatures. The spectrum shown in figure 10 was obtained for the vibrational and rotational temperatures $T_v \sim 10^4$ K and $T_r \sim 2.5 \times 10^3$ K respectively. Similar spectra can be obtained in relatively wide ranges of the temperatures $T_v \sim 0.8\text{--}1.2 \times 10^4$ K and $T_r \sim 2\text{--}3 \times 10^3$ K. To obtain better temperature estimations, a higher spectral resolution is required. In such

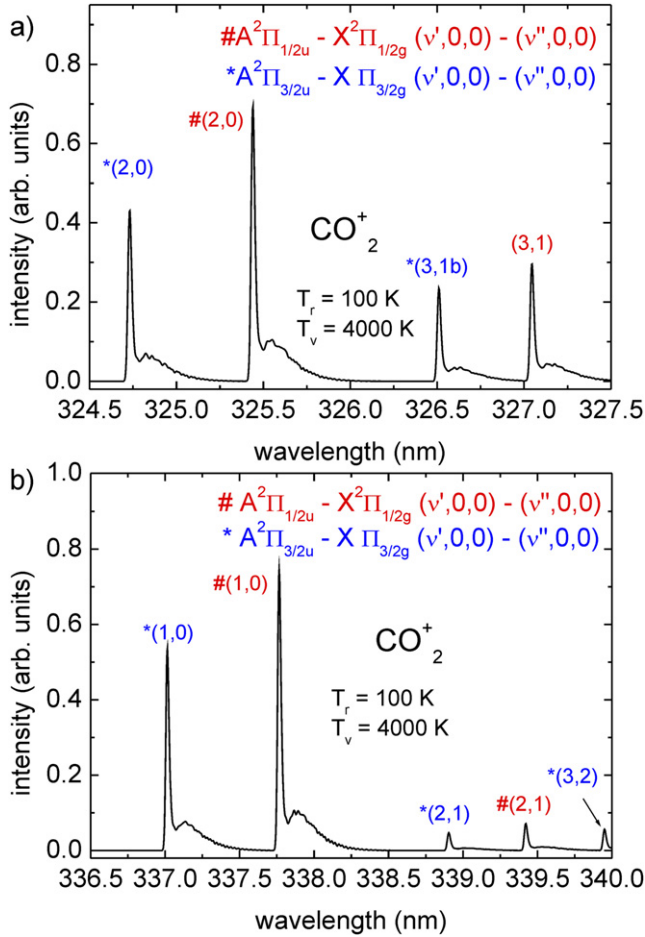


Figure 8. Spectra obtained from numerical simulations of the CO_2^+ emission, using the PGOPHER code. The spectra correspond to the Fox–Duffendack–Barker ($A^2\Pi_u-X^2\Pi_g$) system, recorded for the EUV induced plasmas using the irradiation system based on the NL 303 HT laser (figures 6(b) and (c)).

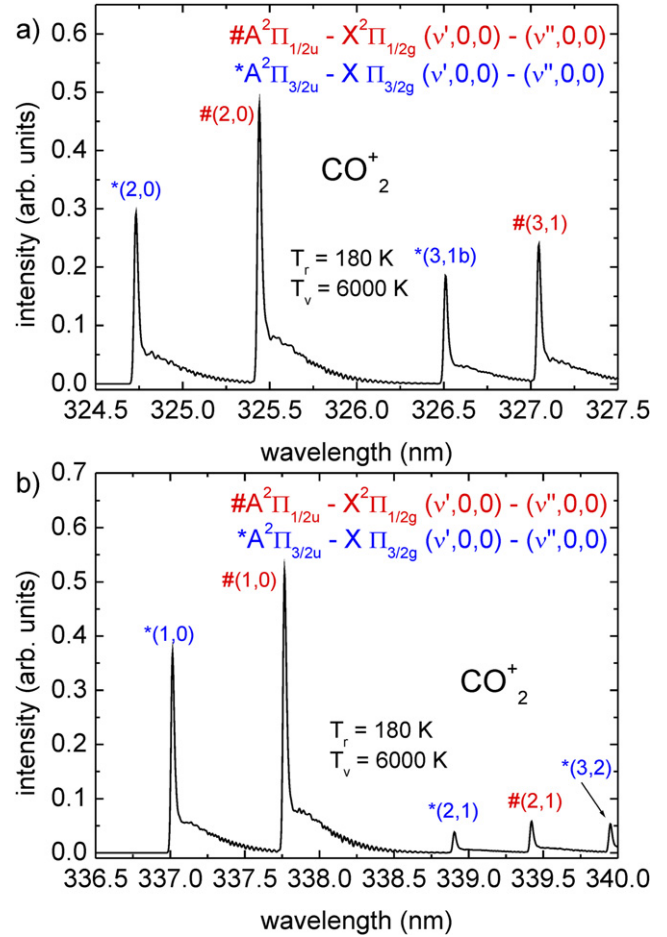


Figure 9. Spectra obtained from numerical simulations of the CO_2^+ emission, using the PGOPHER code. The spectra correspond to the Fox–Duffendack–Barker ($A^2\Pi_u-X^2\Pi_g$) system, recorded for the EUV induced plasmas using the irradiation system based on the NL 129 laser system (figures 6(e) and (f)).

Table 1. Origins and rotational constants concerning the Fox–Duffendack–Barker ($A^2\Pi_u-X^2\Pi_g$) system.

	$X^2\Pi_{1/2g}$ ($\nu'', 0, 0$)	$X^2\Pi_{3/2g}$ ($\nu'', 0, 0$)	$A^2\Pi_{1/2g}$ ($\nu', 0, 0$)	$A^2\Pi_{3/2g}$ ($\nu', 0, 0$)
Origins E (cm^{-1})				
$\nu'' = 0$	640.0	620.0	$\nu' = 1$ 30242.3	30287.2
$\nu'' = 1$	1906.7	1908.3	$\nu' = 2$ 31363.7	31410.4
$\nu'' = 2$	3162.6	3119.0	$\nu' = 3$ 32480.1	32530.8
			$\nu' = 4$ 33592.5	33652.0
Rotational constants B (cm^{-1}) [40]				
B_0	0.3804	0.3796	B_1 0.3492	0.3475
B_1	0.3803	0.3784	B_2 0.3482	0.3466
B_2	0.3793	0.3769	B_3 0.3475	0.3457
			B_4 0.3466	0.3453

a case the detailed band structures would be recorded. In our experiments, only envelopes of rotational lines were obtained.

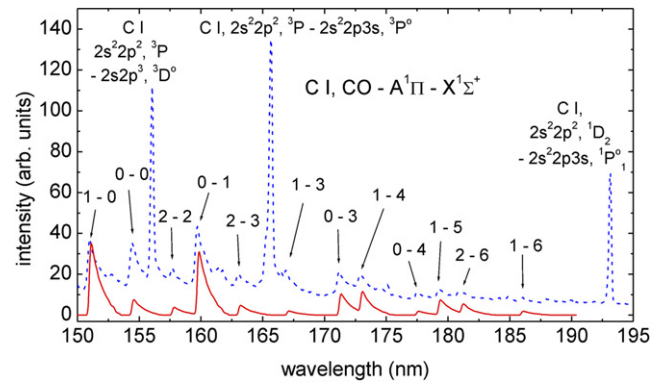


Figure 10. Experimental (dashed line) spectrum of the EUV induced plasma, containing the CI emission lines together with the CO molecular bands, of the $A^1\Pi-X^1\Sigma^+$ system. The corresponding molecular spectrum obtained from numerical simulations (solid line) was included.

4. Discussion of the results

Small portions of CO₂ gas injected into the interaction region with intense EUV pulses were ionized and low temperature plasmas were produced. The EUV pulses were delivered using LPP sources of different parameters. The essential difference concerned the EUV fluence in the interaction region. The maximum fluence measured in the second system (employing the NL129 laser) was 7 times higher compared to the first system. Despite this difference, plasmas induced in both cases contained the same atomic or molecular species. Spectral measurements performed in the VUV–VIS range revealed the presence of singly charged CII ions, CI, OI atoms, CO molecules, and CO₂⁺ molecular ions. The energy of the EUV photons or photoelectrons was sufficient for the creation of any of these species. The highest photon or electron energy was necessary for the creation of CII ions (ionization potential 11.26 eV). This is much lower than the energies of the EUV photons. In this sense, the creation of these species is not dependent on the EUV fluence. On the other hand, the EUV fluence affects the relative intensities of the emission spectral lines, hence, spectral distributions in various wavelength ranges. It can be noticed from the VUV spectra shown in figure 7(b), that an intensity of the line corresponding to single charged carbon ions (CII), in respect to the other lines, especially CI lines, is much higher. An intensity ratio of two adjacent lines CI at $\lambda = 132.9$ nm and CII at $\lambda = 133.5$ nm is 3.9. The corresponding value determined from the spectrum shown in figure 7(a), recorded using the low energy system, is 1.3. In fact, each of the ‘lines’ is composed of a few overlapping spectral lines due to the relatively low resolution of the spectrograph. For this reason, the exact ratios of CII to CI populations cannot be determined. On the other hand, the ratio of relative contributions of the CII ions in plasmas driven by both systems can be estimated as 3:1.

The increase of the EUV fluence affected also the molecular spectra, recorded either in the UV or VUV range. It concerned especially shapes of envelopes of rotational lines. According to the simulations, these differences are mainly connected with the rotational temperatures. Usually, the rotational temperature corresponds to the neutral gas temperature in different types of plasmas. Gases irradiated in our systems are strongly cooled down due to a free expansion into the vacuum chamber. Hence, the rotational temperature is usually very low, far below 0 °C. During irradiation, the temperature can increase due to collisions with photo- and secondary electrons. The increase is, however, not very strong due to a large difference between the electron and molecular masses. For this reason, the rotational temperatures of CO₂⁺ molecular ions are very low ~ 100 K estimated for plasmas produced using the first (low energy) system and ~ 180 K using the second system. On the other hand, rotational temperature determined based on spectra originating from CO molecules is over an order of magnitude higher. This can be explained, taking into account that the formation of CO₂⁺ molecular ions is connected with the release of an electron, while the formation of CO species is connected with the dissociation of CO₂ molecules. Due to the energy and momentum conservation laws, an electron released due to

ionization, carries almost the entire energy E delivered to the molecule minus the ionization potential I : $(\sim (E - I)\frac{m_e}{m_e})$. In the case of the dissociation of a CO₂ molecule, the resulting products—CO and O have masses of the same order, hence, the CO molecule carries a significant part of the energy.

The spatio-temporal measurements indicate that a lifetime of the EUV induced plasma is significantly longer comparing to the duration of the driving EUV pulse. The FWHM of a time profile of the EUV pulse shown in figure 3 is $\tau_{\text{EUV}} = 8.2$ ns, while the FWHM measured for the CO₂-based plasma emission exceeds 30 ns. The emission, however, is over an order of magnitude longer and decreases to 10% of the maximum value during 300 ns. It should be pointed out, that the gas can be photoionized only during a short time corresponding to the duration of the driving pulse. Further ionization is possible due to collisional processes driven by photoelectrons.

The time corresponding to the electron impact ionization phase can be estimated from the formula $\tau = (n_{\text{CO}_2}\sigma v_e)^{-1}$, where σ is the total ionization cross-section for CO₂ molecules, v_e —the electron velocity and n_{CO_2} —CO₂ molecular density. Average energies of the photoelectrons can be roughly estimated to ~ 80 eV, hence, $v_e \approx 5 \times 10^8$ cm s⁻¹. The ionization cross-section is $\sigma = 3 \times 10^{-16}$ cm² [45], the question is about the gas density. To some extent, the density can be estimated from the spatial profile of the streak images. The emission comes from a relatively large area exceeding even the spatial range of the recording system, equal to 9 mm. The FWHM of the emission region is 6 mm and the spatial profile is more or less symmetrical. It means that the EUV absorption was not very strong and a significant part of the driving radiation passed through the gas, not affected. From the transmission calculations, based on the x-ray database [46], assuming that no more than 50% of the EUV radiation was absorbed, it was estimated that the gas density did not exceed 1% of the atmospheric density $n_{\text{CO}_2} \sim 10^{17}$ cm⁻³. In this case, the time corresponding to the collisional ionization phase is very short $\tau \approx 70$ ps. It cannot be responsible for the long duration of the optical emission. On the other hand lifetimes of the electronic A²Π_u states in CO₂⁺ molecules were estimated to the value of 100–120 ns [47]. Also, the recombination rate is over an order of magnitude longer comparing to the ionization processes. It means that a significant fraction of the molecules was ionized and excited during the initial, ionization phase with the time duration not exceeding 10 ns which resulted in the fast increase of the optical emission. After that phase, the emission decreased slowly due to the recombination and radiative decay of the excited states.

5. Summary

In this work results of spectral investigations of the EUV induced, low temperature CO₂-based plasmas, are presented. The main goal of experiments was to identify various reactive species present in such plasmas. Spectral measurements indicated for presence of various species, including single charged ions (CII), atoms (CI, OI), CO molecules and CO₂⁺ molecular ions. Plasmas were induced using two irradiation systems of different pulse durations and the EUV fluence in

the interaction region. In both cases, the same species were detected. Some differences concerned relative intensities of spectral lines and spectral distributions of the molecular bands, especially envelopes of rotational lines. Spectral analysis performed with support of the PGOPHER code indicated for different vibrational and rotational temperatures.

Except for spectral measurements, fast imaging using an optical streak camera was performed. Based on this type of investigation, the size of the densest plasma region was estimated and its temporal evolution. It was demonstrated that the plasma lifetime is much longer comparing to the driving EUV pulse. From some rough estimations, it was concluded that the long duration of the optical emission cannot be connected with the electron impact ionization/excitation phase. It is a result of a long duration of the radiative decay of the excited molecules and recombination processes.

Acknowledgments

This work was supported by the National Science Centre, Poland, Grant Agreement No. UMO-2016/23/B/ST7/00949, and partially by European Union's Horizon 2020 Programme (LASERLAB-EUROPE) Grant Agreement No. 871124

Data availability statement

The data that support the findings of this study are available upon reasonable request from the authors.

ORCID iDs

A Bartnik  <https://orcid.org/0000-0002-7555-8426>

References

- [1] Kawashima K and Kitamoto S 1996 *Publ. Astron. Soc. Japan* **48** L113–6
- [2] Ferland G J 2003 *Annu. Rev. Astron. Astrophys.* **41** 517–54
- [3] Peterson W K, Woods T N, Fontenla J M, Richards P G, Chamberlin P C, Solomon S C, Tobiska W K and Warren H P 2012 *J. Geophys. Res.* **117** A05320
- [4] Bailey J E et al 2001 *J. Quant. Spectrosc. Radiat. Transfer* **71** 157
- [5] Cohen D H, MacFarlane J J, Bailey J E and Liedahl D A 2003 *Rev. Sci. Instrum.* **74** 1962
- [6] Fujioka S et al 2009 *Nat. Phys.* **5** 821–5
- [7] Falcon R E et al 2013 *High Energy Density Phys.* **9** 82–90
- [8] Huebner W F, Keady J J and Lyon S P 1992 *Astrophys. Space Sci.* **195** 1–294
- [9] Pavlov A V 2014 *Surv. Geophys.* **35** 259–334
- [10] Dutuit O et al 2013 *Astrophys. J. Suppl. Ser.* **204** 20
- [11] Samson J A R and Stolte W C 2002 *J. Electron Spectrosc. Relat. Phenom.* **123** 265–76
- [12] Gallagher J W, Brion C E, Samson J A R and Langhoff P W 1988 *J. Phys. Chem. Ref. Data* **17** 9–153
- [13] Itikawa Y, Ichimura A, Onda K, Sakimoto K, Takayanagi K, Hatano Y, Hayashi M, Nishimura H and Tsurubuchi S 1989 *J. Phys. Chem. Ref. Data* **18** 23–42
- [14] Watson W S 1972 *J. Phys. B: At. Mol. Phys.* **5** 2292–303
- [15] Bartnik A, Wachulak P, Fiedorowicz H, Fok T, Jarocki R and Szczurek M 2013 *Phys. Plasmas* **20** 113302
- [16] Bartnik A, Fedosejevs R, Wachulak P, Fiedorowicz H, Serbanescu C, Saiz E G, Riley D, Toleikis S and Neely D 2013 *Laser Part. Beams* **31** 195–201
- [17] Bartnik A, Wachulak P, Fiedorowicz H, Jarocki R, Kostecki J and Szczurek M 2013 *Radiat. Phys. Chem.* **93** 9–13
- [18] Cottin H et al 2008 *Adv. Space Res.* **42** 2019–35
- [19] Dobrijevic M and Parisot J P 1995 *Adv. Space Res.* **15** 1–4
- [20] Blitz M A and Seakins P W 2012 *Chem. Soc. Rev.* **41** 6318–47
- [21] van der Horst R M, Beckers J, Osorio E A and Banine V Y 2015 *J. Phys. D: Appl. Phys.* **48** 432001
- [22] van der Horst R M et al 2016 *J. Phys. D: Appl. Phys.* **49** 145203
- [23] van der Horst R M, Osorio E A, Banine V Y and Beckers J 2016 *Plasma Sources Sci. Technol.* **25** 015012
- [24] van der Horst R M, Beckers J, Nijdam S and Kroesen G M W 2014 *J. Phys. D: Appl. Phys.* **47** 302001
- [25] van de Ven T H M, Reefman P, de Meijere C A, van der Horst R M, van Kampen M, Banine V Y and Beckers J 2018 *J. Appl. Phys.* **123** 063301
- [26] Bartnik A, Skrzeczanowski W, Czwartos J, Kostecki J, Fiedorowicz H, Wachulak P and Fok T 2018 *Phys. Plasmas* **25** 063508
- [27] Czwartos J, Budner B, Bartnik A, Wachulak P, Fiedorowicz H and Mierczyk Z 2020 *Materials* **13** 4466
- [28] Bartnik A, Skrzeczanowski W, Fiedorowicz H, Wachulak P and Fok T 2018 *Laser Part. Beams* **36** 76–83
- [29] Lech A, Butruk-Raszeja B A, Ciach T, Lawniczak-Jablonska K, Kuzmiuk P, Bartnik A, Wachulak P and Fiedorowicz H 2020 *Int. J. Mol. Sci.* **21** 9679
- [30] Western C M 2017 *J. Quant. Spectrosc. Radiat. Transfer* **186** 221–42
- [31] Western C M and Billingham B E 2017 *Phys. Chem. Chem. Phys.* **19** 10222–6
- [32] Bartnik A, Fiedorowicz H, Jarocki R, Kostecki J, Szczurek M and Wachulak P W 2011 *Nucl. Inst. Meth. Phys. Res. A* **647** 125–31
- [33] Wachulak P et al 2017 *Appl. Sci.* **7** 548
- [34] Torrisi A et al 2017 *J. Microsc.* **265** 251–60
- [35] Bartnik A, Skrzeczanowski W, Wachulak P, Saber I, Fiedorowicz H, Fok T and Węgrzyński Ł 2017 Reflective optics for effective collection of x-ray and EUV radiation: use for creation of photoionized plasmas and detection of weak signals *Proc. SPIE 10235, EUV and X-Ray Optics: Synergy between Laboratory and Space V*
- [36] Bartnik A, Lisowski W, Sobczak J, Wachulak P, Budner B, Korczyk B and Fiedorowicz H 2012 *Appl. Phys. A* **109** 39–43
- [37] Simmons J D, Bass A M and Tilford S G 1969 *Astrophys. J.* **155** 345–58
- [38] McCallum J C and Nicholls R W 1972 *J. Phys. B: At. Mol. Phys.* **5** 1417–26
- [39] Kim S J 1999 *Earth Planet Space* **51** 139–45
- [40] McCallum J C and Nicholls R W 1971 *J. Phys. B: At. Mol. Phys.* **4** 1096–101
- [41] Mrozowski S 1941 *Phys. Rev.* **60** 730–8
- [42] Mrozowski S 1942 *Phys. Rev.* **62** 270–9
- [43] Western C M 2017 *J. Quant. Spectrosc. Radiat. Transfer* **186** 221–42 <http://pgopher.chm.bris.ac.uk>
- [44] Huber K P and Herzberg G H 2021 Constants of diatomic molecules *NIST Chemistry WebBook, NIST Standard Reference Database Number 69*, ed P J Linstrom and W G Mallard (Gaithersburg, MD: National Institute of Standards and Technology) <https://webbook.nist.gov/cgi/cbook.cgi?ID=C630080&Units=SI&Mask=1000#Diatomic> (Data prepared by Jean W Gallagher and Russell D Johnson III)
- [45] Deutsch H, Becker K, Matt S and Märk T D 2000 *Int. J. Mass Spectrom.* **197** 37–69
- [46] Henke B L, Gullikson E M and Davis J C 1993 *At. Data Nucl. Data Tables* **54** 181–342
- [47] Herran C, Arqueros F and Campos J 1983 *J. Mol. Spectrosc.* **97** 244–7